AGU PUBLICATIONS

Geophysical Research Letters

RESEARCH LETTER
10.1002/2016GL072223

Key Points:
- AMOC strength is proportional to mean salinity
- PMOC strength declines with mean salinity
- Scaling laws for the overturning circulation explain these dependencies

Supporting Information:
- Supporting Information S1

Correspondence to:
B. B. Cael,
bcaelb@mit.edu

Citation:
Cael, B. B., and R. Ferrari (2017), The ocean's saltiness and its overturning, *Geophys. Res. Lett.*, *44*, doi:10.1002/2016GL072223.

Received 2 DEC 2016
Accepted 7 FEB 2017
Accepted article online 9 FEB 2017

The ocean's saltiness and its overturning

B. B. Cael[1,2] and Raffaele Ferrari[1]

[1]Department of Earth, Atmosphere, and Planetary Sciences, Massachusetts Institute of Technology, Cambridge, Massachusetts, USA, [2]Department of Physical Oceanography, Woods Hole Oceanographic Institution, Woods Hole, Massachusetts, USA

Abstract Here we explore the relationship between the mean salinity $\bar{S}$ of the ocean and the strength of its Atlantic and Pacific Meridional Overturning Circulations (AMOC and PMOC). We compare simulations performed with a realistically configured coarse-grained ocean model, spanning a range of mean salinities. We find that the AMOC strength increases approximately linearly with $\bar{S}$. In contrast, the PMOC strength declines approximately linearly with $\bar{S}$ until it reaches a small background value similar to the present-day ocean. Well-established scaling laws for the overturning circulation explain both of these dependencies on $\bar{S}$.

1. Introduction

The Atlantic meridional overturning circulation (AMOC) transports cold water masses formed through convection in the North Atlantic southward at depth, balanced by a northward resupply of warm surface waters [*Wolfe and Cessi*, 2014]; no such circulation exists in the Pacific, but paleoevidence suggests that deep water formation has occurred in the North Pacific in the past [*Okazaki et al.*, 2010]. The asymmetry in overturning between these two basins has been the subject of extensive research because of its important consequences for ocean circulation and the transport of heat and carbon [*Vallis*, 2012] and is usually attributed to interbasin differences in evaporation/precipitation [*Warren*, 1983; *Emile-Geay et al.*, 2003; *Nilsson et al.*, 2011], though there is no consensus as to why deep water formation is only seen in the Atlantic. Here we investigate the role of *mean salinity* on this overturning asymmetry. Mean salinity may have an impact because salinity affects the density-temperature relationship [*Roquet et al.*, 2015], because seawater density is sensitive to salinity at high latitudes where $T \approx 0$°C [*Timmermans and Jayne*, 2016] and because salinity variations scale with mean salinity [*Cullum et al.*, 2016] as salinity variations are due to evaporation, precipitation, and other water injection/removal events rather than direct input of salts.

We approach the relationship between ocean mean salinity and the MOCs in the spirit of a geophysical fluid dynamics problem, exploring the dependency of their strengths on the mean salinity through a range of mean salinities. This dependency may have relevance for past climates; paleoevidence suggests that the mean salinity of the world ocean has varied widely on geological timescales, due both to large-scale extraction of water to form ice sheets and to changes in the total salt content from imbalances in salt deposit and extraction [*Hay et al.*, 2006]. Salinity during Snowball Earth has recently been shown to dominate the density structure, in part because the mean salinity, expected to have exceeded 50 g/kg as prescribed in the simulations, would have caused enhanced density variations [*Jansen*, 2016]. Simulations of an ocean in an idealized configuration suggested that inclusion of salinity increases the strength of the MOC [*Wolfe and Cessi*, 2014]. The combination of this geological and simulation evidence suggests the mean salinity affects and possibly has affected circulation patterns in the ocean's past, but the dependence of ocean circulation features on the mean salinity has not been explored. Additionally, this dependency may have relevance for exoplanet circulations; changing the mean salinity in box models has been shown to change meridional heat transport because different circulation patterns can emerge, with hypothesized implications for exoplanet habitability [*Cullum et al.*, 2016].

We also note that transient sensitivity simulations in a coupled ocean-atmosphere model where an additional 35 g/kg of salt was added uniformly to the ocean showed a ~1/2°C increase in globally averaged sea surface temperature and a temporarily weakened AMOC [*Williams et al.*, 2010]. However, here we are interested in equilibrium responses of the overturning circulation; caution should be taken not to conflate transient and

equilibrium MOC responses to perturbations, which can often be in opposite directions [e.g., *Stouffer and Manabe*, 2003].

We perform a suite of experiments with a coarse-grained, but realistic, ocean model, compare the resulting MOC strengths at equilibrium and evaluate the relationship between mean salinity and MOC strength using simple physical arguments. We find that the AMOC strengthens and the analogous upper overturning cell in the Pacific (Pacific Meridional Overturning Circulations, PMOC) weakens with increasing $\bar{S}$ and that these dependencies are consistent with the predominant theory for the overturning circulation [*Nikurashin and Vallis*, 2012; *Wolfe and Cessi*, 2014]. We also analyze the effect of implementing lower-order equations of state for a simulation with the present-day mean salinity and a simulation with $\bar{S} = 0$.

2. Materials and Methods

2.1. Numerical Model

As analytical solutions of the equations governing oceanic flow are not available for realistic ocean geometries, and comprehensive observations are only available for the ocean at its present-day salinity, numerical simulations are required to study the dependency of the AMOC and PMOC on the ocean's mean salinity. We use the letter ξ to represent ratio of the mean salinity of a given simulation with the present-day ocean mean salinity of $\bar{S} \approx 34.7$ g/kg [*Wunsch*, 2014]; i.e., $\xi := \bar{S}/34.7$. For these numerical experiments, we use a global rigid lid configuration of the Massachusetts Institute of Technology General Circulation Model (MITgcm) [*Marshall et al.*, 1997] at 2.8° horizontal resolution with 15 nonuniform vertical levels. Global realistic ocean bathymetry is derived from *Sloss* [1988]. The mesoscale eddy field is parameterized by using the *Gent and McWilliams* [1990] scheme with an eddy diffusivity of 1000 m^2/s and a diapycnal diffusivity of 5×10^{-5} m^2/s. Momentum is dissipated using a Laplacian viscosity with horizontal coefficient of 5×10^5 m^2/s and a vertical coefficient of 1×10^{-3} m^2/s. Tracers are advected using a flux-limited second-moment scheme. Enhanced mixing at boundary layers and in low stratification is implemented using a κ profile parameterization mixing scheme [*Large et al.*, 1994]. Wind stress forcing is taken from *Trenberth et al.* [1989]. Heat fluxes are imposed by restoring to a monthly varying effective atmospheric temperature as suggested by *Haney* [1971], on a timescale of 60 days over 25 m (see Figure S1b in the supporting information) [*Levitus and Boyer*, 1994b]. Freshwater forcing is imposed as a relaxation to a prescribed, monthly varying sea surface salinity field [*Levitus and Boyer*, 1994a] (see Figure S1a) on a 90 day timescale over 25 m, rather than as an evaporation-precipitation flux, to avoid model drift. The model time step is 12 h. All experiments described below are run to equilibrium, and diagnostics are then computed for the last century of model output.

2.2. Reference Simulation and Overturning Stream Function

The equilibrium state of the reference experiment (experiment *a* in Table 1; see below) mirrors the large-scale time-mean circulation patterns of the present-day ocean (see Figure S2), with a comparable vertical structure, midlatitude gyres in each basin with tens of Sverdrup (Sv) of transport, and a strong Antarctic Circumpolar Current with ~150 Sv transport through the Drake Passage, consistent with observations [*Wunsch*, 2014; *Gille*, 2003]. To quantify the overturning circulation for this and other experiments, we introduce the overturning stream function.

The overturning stream functions ψ_A and ψ_P, in units of Sverdrups (1 Sv = 10^6 m^3/s), represent each basin's zonally integrated net volume transport as an integral [*Wunsch*, 2014]. They are defined here such that

$$V(y,z) + V_{\mathrm{GM}}(y,z) = -\partial_z \psi_{A,P}(y,z),$$

$$W(y,z) + W_{\mathrm{GM}}(y,z) = \partial_y \psi_{A,P}(y,z),$$

where capital letters on the left-hand side are zonal integrals of meridional velocity v, vertical velocity w, and the Gent-McWilliams eddy-induced transport velocities v_{GM} and w_{GM} [*McWilliams*, 2006], over the zonal extents of the Atlantic and Indo-Pacific basins (for the respective subscripts $\cdot_A$, $\cdot_P$) at latitude y and depth z. For each experiment described below, ψ_A and ψ_P are computed for the time-averaged velocity field for the last century of model output. The positive maxima of ψ_A and ψ_P (north of 30° N, to avoid the large upper ocean wind-driven cells in the subtropics), which represent clockwise circulations, serve as metrics for the strength of the AMOC and PMOC.

The overturning stream functions $\psi_{A,P}$ from the reference experiment also mirror the structure and magnitude of the overturning circulation in the present-day ocean as estimated by *Lumpkin and Speer* [2007]

Table 1. Description of Experiments: Simulation Letter Designation, Ratio of Mean Salinity for the Simulation to That of the Reference Experiment (ξ), and Equation of State (EoS)

Letter	ξ	EoS
a	1	polynomial
b	0	polynomial
c	1/15	polynomial
d	1/6	polynomial
e	1/3	polynomial
f	2/3	polynomial
g	3/2	polynomial
h	3	polynomial
i	1	JMD95Z
j	1	linear
k	0	quadratic

(see Figure S3a). In the Atlantic, a clockwise AMOC circulation of 19 Sv is confined to the upper ~2 km, with convection occurring at the highest Atlantic latitudes. A weaker 12 Sv counterclockwise circulation associated to convection around Antarctica can be seen below the AMOC. This two-cell zonally averaged circulation compares well with observations [*Lumpkin and Speer*, 2007; *Talley*, 2013].

The PMOC is far weaker at 3 Sv and largely confined to the upper kilometer of the Pacific, also comparable to observations [*Talley*, 2013].

2.3. Experiments

Eleven experiments were conducted using the numerical model described above; see Table 1. Collectively, the suite of experiments tests for the dependence of AMOC and PMOC strength on ocean mean salinity and on the adequacy of lower-order equations of state to reproduce large-scale features of the ocean circulation in present-day conditions and the zero-salt limit. Experiment *a* serves as a reference experiment, using realistic salinity forcing and a nonlinear equation of state which is an accurate 10-term Taylor expansion about the mean (S, T, and P) at each depth level [*Bryan and Cox*, 1972]. Experiments *b*–*h* are identical to *a* except that the salinity initial conditions and surface forcing are multiplied by a constant factor ξ between 0 and 3. Salinity is shifted in this way to maintain relative salinity differences while changing the mean salinity [*Cullum et al.*, 2016].

Experiment *i* replicates experiment *a* but uses a different nonlinear equation of state with 12 terms per depth level, to verify that results are not sensitive to the specific implementation of equation of state nonlinearities [*Jackett and McDougall*, 1995]. Experiment *j* approximates the equation of state in experiment *a* with a linearization about the mean salinity and temperature of the equilibrated state of experiment *a*, resulting in a constant temperature expansion coefficient of $\alpha = 1.47 \times 10^{-4}$°C^{-1} and a constant saline density coefficient [*Wunsch*, 2014] of $\beta = 7.50 \times 10^{-4}$ kg/g, to test the adequacy of a linear equation of state to reproduce large-scale ocean circulation patterns in a model configured as above and approximating present-day ocean conditions.

Investigating the habitability of exoplanets, *Cullum et al.* [2016] used a box model to test for the impact of mean salinity on an idealized ocean circulation. As freshwater at surface pressure has a nearly quadratic equation of state with respect to temperature, they used a quadratic function for $\rho(T)$ to test the case where $\bar{S} = 0$. This formulation may not be appropriate for freshwater in an ocean interior, however, where thermobaric terms become important (see Figure S4). Thus, to test for the impact of these thermobaric terms on large-scale circulation patterns in the $\bar{S} = 0$ case, experiment *k* uses a quadratic equation of state $\rho = \rho_o + \alpha_1 T - \alpha_2 T^2$, with $\rho_o = 999.9$ kg m^{-3}, $\alpha_1 = 0.044$ kg m^{-3}°C^{-1}, and $\alpha_2 = 0.0054$ kg m^{-3}°C^{-2}, which is a highly accurate approximation of the density-temperature relationship at zero salinity and atmospheric pressure across the full range of ocean surface temperatures (root-mean-square error (RMSE) = 0.0165 kg m^{-3}) but neglects thermobaric terms.

3. Results

3.1. MOC's Dependence on ξ

We compare positive maxima of ψ_A and ψ_P for experiments *a*–*h* in Figure 1. The AMOC strength (maximum of ψ_A) increases monotonically with ξ. The AMOC-ξ relationship is approximately linear ($\max\{\psi_A\} \approx 6.7\xi + 13$ Sv; $r^2 = 0.988$; and RMSE = 0.8) , such that in the zero-salinity limit the AMOC weakens to 13 Sv of transport and increases by 6.7 Sv for each unit increase of ξ; equivalently, the AMOC strength increases by 0.19 Sv for each unit increase (in g/kg) of $\bar{S}$.

The linear increase of ψ_A with ξ is consistent with general theory for the strength of the AMOC and with simulations in idealized ocean configurations. For an adiabatically dominated overturning such as the AMOC,

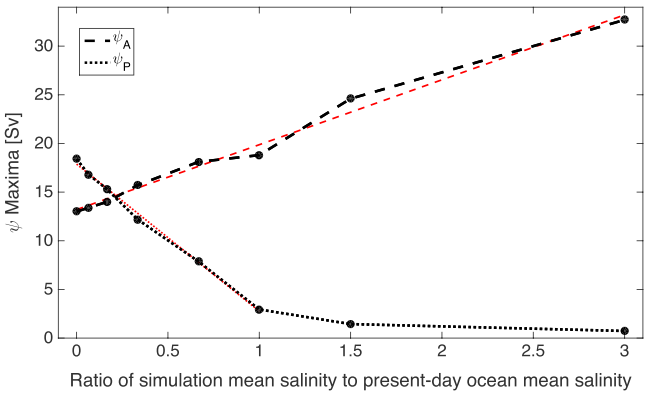

Figure 1. Basin overturning stream function maxima as a function of the ratio of mean salinity (ξ) for simulations *a*–*h*. Black dashed and dotted lines correspond to Atlantic and Pacific MOC's, respectively. Red dashed and dotted lines are estimated linear relationships ($\max \psi_A \approx 6.7\xi + 13$, $r^2 = 0.988$, and RMSE = 0.8, and for $\xi \leq 1$, $\max \psi_P \approx 18 - 15\xi$, $r^2 = 0.996$, and RMSE = 0.4).

the strength Ψ is thought to be proportional to the "isopycnal window" Δb, the range of buoyancy over which convection occurs, according to the scaling

$$\Psi \sim \frac{h^2 \Delta b}{f},$$

where h is the depth scale for the overturning and f is the Coriolis parameter at high northern latitudes [*Nikurashin and Vallis*, 2012; *Wolfe and Cessi*, 2014]. The partitioning of Atlantic waters between the AMOC cell and the abyssal Atlantic circulation associated to convection around Antarctica remains fixed across these experiments, keeping h roughly constant. However, the Δb changes across the experiments because the range of salinity over which convection occurs, ΔS, increases with the mean salinity. The ~7 Sv increase in Ψ per unit increase in ξ seen in the experiments is also predictable from the above scaling. If we take from the reference simulation $\Delta S \sim 0.1$ g/kg, and take the depth of the positive ψ_A maximum for $h \sim 1$ km, given the characteristic magnitudes $\beta \sim 7 \times 10^{-4}$ kg/g, $g \sim 10$ m/s^2, and $f \sim 10^{-4}$ s^{-1}, the change ($\delta\Psi$) in Ψ from a unit change ($\delta\xi = 1$) in ξ should be

$$\Psi \sim \frac{h^2 \Delta b}{f} \quad \longrightarrow \quad \delta\Psi \sim \frac{h^2 g \beta \Delta S}{f} \delta\xi \sim 7 \text{ Sv}.$$

In contrast, PMOC strength (maximum of ψ_P) decreases monotonically with ξ. The PMOC strength increases to 18.4 Sv in the zero-salinity limit and decreases to 1.8 Sv when $\xi = 3$. For $\xi > 1$; the PMOC effectively vanishes to a small background value, but when $\xi \leq 1$, the PMOC-ξ relationship is approximately linear ($\max \psi_P \approx 18 - 15\,\xi$; $r^2 = 0.996$; and RMSE = 0.4).

The PMOC behavior can be interpreted within the same scaling framework given for the AMOC. Even though the North Pacific experiences cold temperatures, it exhibits and is stratified by a persistent halocline [*Gargett*, 1991]. Decreasing mean salinity weakens this halocline because freshwater fluxes result in proportionately weaker buoyancy fluxes, thus a weaker stratification. Weaker stratification from a sufficiently decreased $\bar{S}$ can allow enhanced convection across a range of isopycnals, thus increasing Δb. In contrast, when $\bar{S}$ is large enough to shut down convection in the North Pacific via a strong enough halocline, Δb vanishes, and any clockwise PMOC associated with high-latitude convection must be balanced by a diffusive upwelling within the basin. In the above scaling framework, this diffusive upwelling scales as $\Psi \sim \kappa \mathcal{A}/h$, where κ is the vertical diffusivity and $\mathcal{A}$ is the area of the basin [*Munk*, 1966]. Such scalings typically produce Ψ estimates on the order of a few Sverdrups [*Nikurashin and Vallis*, 2012], consistent with observations [*Talley*, 2013] and the $\xi \geq 1$ experiments.

3.2. Lower-Order Equations of State

We compare experiments *a*, *i*, and *j* to test the importance of nonlinearities in the equation of state for the case when $\xi = 1$. The AMOC and PMOC for experiments *a* and *i* are effectively indistinguishable, with an AMOC maximum of 18.8 Sv and a PMOC maximum of 2.9 Sv for both experiments, and nearly identical structure both meridionally and in depth (see Figures S3a and S3i). This suggests that the particular representation of equation of state nonlinearities does not affect these overturnings. Interestingly, the AMOC and PMOC for experiments *a* and *j* are also nearly indistinguishable; experiment *j* has an AMOC maximum of 19.7 Sv and a PMOC maximum of 2.4 Sv, and moreover, the overall structure of both MOCs are strikingly similar between the two experiments (see Figures S3a and S3j). The quantitative differences in AMOC and PMOC strength between experiments *a* and *j* are smaller than present measurement uncertainties for the strength of each circulation [*Talley et al.*, 2003].

Even though the equilibrium dynamics of these experiments are similar, substantial quantitative differences exist in the distribution of temperature and salinity between the two (see Figure S5); the most abundant water mass in experiment *j* has a salinity of ∼0.26 g/kg lower than that of experiment *a* and a potential temperature of ∼1.8°C lower. These quantitative differences are consistent with those found by *Roquet et al.* [2015], who found that changing from a nonlinear equation of state to a linear one in their simulations produced a mean salinity change of −0.2 g/kg and a mean temperature change of −1.9°C. This suggests that for the present-day ocean mean salinity, i.e., $\xi = 1$, while nonlinearities in the equation of state may not be necessary to approximate the AMOC or PMOC, the water mass distributions and the characteristics of the waters advected by these circulations are affected by these nonlinearities [*Nycander et al.*, 2015].

We also compare experiments *b* and *k* to test the importance of nonlinearities in the equation of state other than the temperature-quadratic term α_2 for the case when $\xi = \bar{S} = 0$. Experiment *k* produces a substantially weaker AMOC than experiment *b*, 6.7 Sv versus 13.0 Sv. Additionally, the PMOC in experiment *k* is structured entirely differently, extending down to the ocean bottom, whereas in all other experiments the PMOC is confined to the upper ∼2 km (see Figures S3b and S3k). Experiment *k* also produces a substantially weaker Antarctic Circumpolar Current, with 68 Sv of transport through the Drake Passage; experiments *a*–*j* all produces similar Drake Passage transports of ∼150 Sv, consistent with observations [*Gille*, 2003]. This suggests that an equation of state neglecting thermobaric effects is insufficient to approximate accurately large-scale circulation features in the limit of zero salinity. In the present-day ocean, thermobaric effects are thought to play an important role in high latitude convection [*Oliver and Tailleux*, 2013; *Adkins et al.*, 2005]. For freshwater, the density-temperature relationship changes with increasing pressure, strikingly similar to the effect of increasing salinity for saltwater at surface pressure (see Figure S4). Increasing pressure has a nearly equivalent impact on the density-temperature relationship as increasing salinity, as both weaken the influence of hydrogen bonding at low temperatures and thus the freshwater density maximum at 4°C [*Thurman*, 1988]. Figure S4 demonstrates that when $\xi = 0$, a quadratic equation of state is only accurate for surface waters. As the MOC is a property of the ocean interior, spurious overturnings are likely to result from simulations neglecting thermobaric terms by using a quadratic equation of state for the $\xi = 0$ case.

4. Discussion

We have used numerical simulations to explore the dependence of the overturning circulation on the ocean's mean salinity. The AMOC increases linearly with mean salinity, while the PMOC decreases linearly until it asymptotes to a small background value. Increasing $\bar{S}$ results in opposite effects on the two overturnings. This is because in the Atlantic an increase in mean salinity leads to an increased isopycnal window Δb, whereas in the Pacific an increase in mean salinity leads to a stronger halocline and thus a smaller isopycnal window due to the shutdown of convection.

The similarity between experiments *a* and *j* indicates that a linear equation of state is sufficient in a model configured as above to approximate the large-scale time-mean circulation accurately, well within current measurement uncertainty [*Talley et al.*, 2003], but that equation of state nonlinearities affect water mass characteristics. This is likely dependent on model configuration, and we note that a linear equation of state is unlikely to capture regional circulations in uniformly low-temperature oceans accurately [*Timmermans and Jayne*, 2016].

The model used herein is not an appropriate candidate to investigate precise, quantitative differences resulting from changes in mean salinity. A higher-resolution, coupled atmosphere-ice-ocean model is necessary to fully capture the effects of mean salinity and varied equations of state on the ocean circulation and water mass distribution [*Roquet et al.*, 2015]. All such models are approximate integrals of partial differential equations subject to a series of strong assumptions. However, as the model reproduces qualitative features of the circulation for multiple equations of state, and simple physical arguments can explain the difference between experiments, the model becomes a compelling tool to illustrate the qualitative influence of a mean salinity for the overturning. A key objective of physical oceanography and geophysical fluid dynamics alike is to understand what underlies oceanic movement [*McWilliams*, 2006; *Wunsch*, 2014]. Here we have shown that the mean salinity of the ocean is a constraint on the strength of its overturning cells.

Acknowledgments
It is a pleasure to thank Jon Lauderdale for indispensable assistance configuring the MITgcm. This material is based upon work supported by the National Science Foundation Graduate Research Fellowship Program under grant 2388357 and the National Science Foundation, awards OCE-1315201 and OCE-1536515.

References

Adkins, J. F., A. P. Ingersoll, and C. Pasquero (2005), Rapid climate change and conditional instability of the glacial deep ocean from the thermobaric effect and geothermal heating, *Quat. Sci. Rev.*, *24*(5), 581–594.
Bryan, K, and M. D. Cox (1972), An approximate equation of state for numerical models of ocean circulation, *J. Phys. Oceanogr.*, *2*(4), 510–514.
Cullum, J., D. P. Stevens, and M. M. Joshi (2016), Importance of ocean salinity for climate and habitability, *Proc. Nat. Acad. Sci.*, *113*(16), 4278–4283.
Emile-Geay, J., et al. (2003), Warren revisited: Atmospheric freshwater fluxes and "Why is no deep water formed in the North Pacific", *J. Geophys. Res.*, *108*, 3178, doi:10.1029/2001JC001058.
Gargett, A. E. (1991), Physical processes and the maintenance of nutrient-rich euphotic zones, *Limnol. Oceanogr.*, *36*, 1527–1545.
Gent, P. R., and J. C. McWilliams (1990), Isopycnal mixing in ocean circulation models, *J. Phys. Oceanogr.*, *20*(1), 150–155.
Gille, S. T. (2003), Float observations of the Southern Ocean. Part I: Estimating mean fields, bottom velocities, and topographic steering, *J. Phys. Oceanogr.*, *33*(6), 1167–1181.
Haney, R. L. (1971), Surface thermal boundary condition for ocean circulation models, *J. Phys. Oceanogr.*, *1*(4), 241–248.
Hay, W. W., et al. (2006), Evaporites and the salinity of the ocean during the Panerozoic: Implications for climate, ocean circulation and life, *Palaeogeogr. Palaeoclimatol. Palaeoecol.*, *240*(1), 3–46.
Jackett, D. R., and T. J. McDougall (1995), Minimal adjustment of hydrographic profiles to achieve static stability, *J. Atmos. Oceanic Technol.*, *12*(2), 381–389.
Jansen, M. (2016), The turbulent circulation of a Snowball Earth ocean, *J. Phys. Oceanogr.*, *46*(6), 1917–1933.
Large, W. G., J. C. McWilliams, and S. C. Doney (1994), Oceanic vertical mixing: A review and a model with a nonlocal boundary layer parameterization, *Rev. Geophys.*, *32*(4), 363–403.
Levitus, S., and T. Boyer, (1994a), World Ocean Atlas 1994, volume 3: Salinity, Tech. Rep., NOAA Atlas NESDIS 3, U.S. Dep. of Commerce, Washington, D. C.
Levitus, S., and T. Boyer, (1994b), World Ocean Atlas 1994, volume 4: Temperature, Tech. Rep., NOAA Atlas NESDIS 4, U.S. Dep. of Commerce, Washington, D. C.
Lumpkin, R., and K. Speer (2007), Global ocean meridional overturning, *J. Phys. Oceanogr.*, *37*(10), 2550–2562.
Munk, W. H. (1966), Abyssal recipes, *Deep. Sea Res. Oceanogr. Abstr.*, *13*(4), 707–730.
Marshall, J., A. Adcroft, C. Hill, L. Perelman, and C. Heisey (1997), A finite-volume, incompressible Navier Stokes model for studies of the ocean on parallel computers, *J. Geophys. Res.*, *102*(C3), 5753–5766.
McWilliams, J. C. (2006), *Fundamentals of Geophysical Fluid Dynamics*, Cambridge Univ. Press, Cambridge, U. K.
Nikurashin, M., and G. Vallis (2012), A theory of the interhemispheric meridional overturning circulation and associated stratification, *J. Phys. Oceanogr.*, *42*(10), 1652–1667.
Nilsson, J., P. L. Langen, D. Ferreira, and J. Marshall (2011), Ocean basin geometry and the salinification of the Atlantic Ocean, *J. Clim.*, *26*(16), 6163–6184.
Nycander, J., M. Hieronymus, and F. Roquet (2015), The nonlinear equation of state of sea water and the global water mass distribution, *Geophys. Res. Lett.*, *42*, 7714–7721, doi:10.1002/2015GL065525.
Okazaki, Y., et al. (2010), Deepwater formation in the North Pacific during the last glacial termination, *Science*, *329*(5988), 200–204.
Oliver, K. I. C., and R. Tailleux (2013), Thermobaric control of gravitational potential energy generation by diapycnal mixing in the deep ocean, *Geophys. Res. Lett.*, *40*, 327–331, doi:10.1029/2012GL054235.
Roquet, F., G. Madec, L. Broeau, and J. Nycander (2015), Defining a simplified yet "realistic" equation of state for seawater, *J. Phys. Oceanogr.*, *45*(10), 2564–2579.
Sloss, P. W. (1988), *Data Announcement 88-MGG2, Digital Relief of the Surface of the Earth*, NOAA, Natl. Geophys. Data Cent., Boulder, Colo.
Stouffer, R. J., and S. Manabe (2003), Equilibrium response of thermohaline circulation to large changes in atmospheric CO_2 concentration, *Clim. Dyn.*, *20*(7–8), 759–773.
Talley, L. D., J. L. Reid, and P. E. Robbins (2003), Data-based meridional overturning streamfunctions for the global ocean, *J. Clim.*, *16*(19), 3213–3226.
Talley, L. D. (2013), Closure of the global overturning circulation through the Indian, Pacific, and Southern Oceans: Schematics and transports, *Oceanography*, *26*(1), 80–97.
Thurman, H. V. (1988), *Introductory Oceanography* 5th ed., Merrill Publ. Company, Columbus, Ohio.
Timmermans, M., and S. Jayne (2016), The Arctic Ocean spices up, *J. Phys. Oceanogr.*, *46*(4), 1277–1284.
Trenberth, K., J. Olson, and W. Large, (1989), A global wind stress climatology based on ECMWF analyses, *Tech. Rep. NCAR/TN-338+STR*, Natl. Cent. for Atmos. Res., Boulder, Colo.
Vallis, G. K. (2012), *Climate and the Oceans*, Princeton Univ. Press, Princeton, N. J.
Warren, B. (1983), Why is no deep water formed in the Pacific?, *J. Marine Res.*, *41*(2), 327–347.
Williams, P. D., et al. (2010), The role of mean ocean salinity in climate, *Dyn. Atmos. Oceans*, *49*(2), 108–123.
Wolfe, C., and P. Cessi (2014), Salt feedback in the adiabatic overturning circulation, *J. Phys. Oceanogr.*, *44*(4), 1175–1194.
Wunsch, C. (2014), *Modern Observational Physical Oceanography: Understanding the Global Ocean*, Princeton Univ. Press, Princeton, N. J.

[Geophysical Research Letters]

Supporting Information for

[The ocean's saltiness and its overturning]

[B. B. Cael[1,2], Raffaele Ferrari[1]]

[1. Department of Earth, Atmosphere, and Planetary Sciences, Massachusetts Institute of Technology, Cambridge, Massachusetts, USA

2. Department of Physical Oceanography, Woods Hole Oceanographic Institution, Woods Hole, Massachusetts, USA]

Contents of this file

Introduction

Below are the supporting figures S1 through S5. See figure captions for descriptions of each figure.

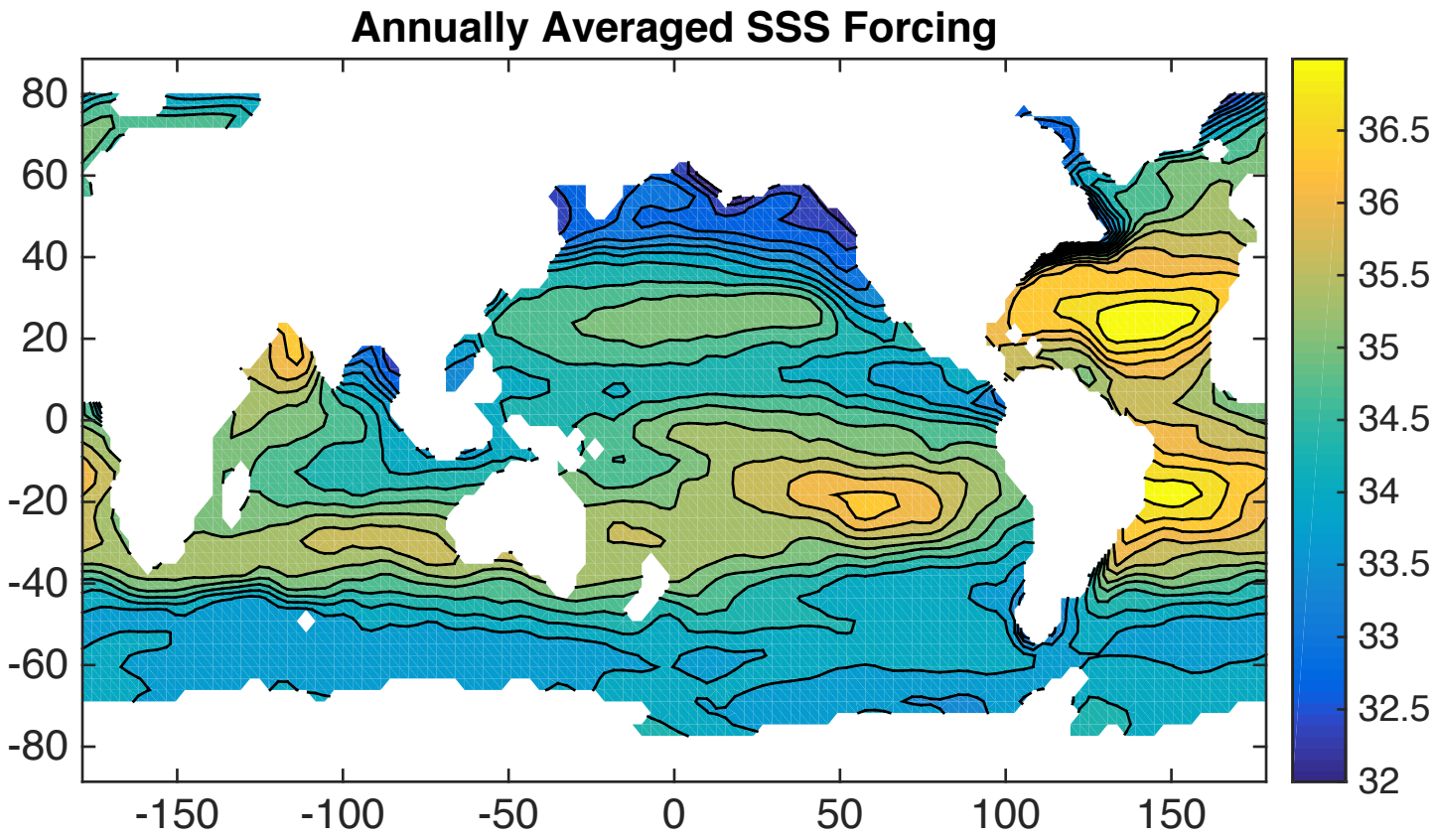
Annually Averaged SSS Forcing
80
60
40
20
0
-20
-40
-60
-80
-150
-100
-50
0
50
100
150
36.5
36
35.5
35
34.5
34
33.5
33
32.5
32

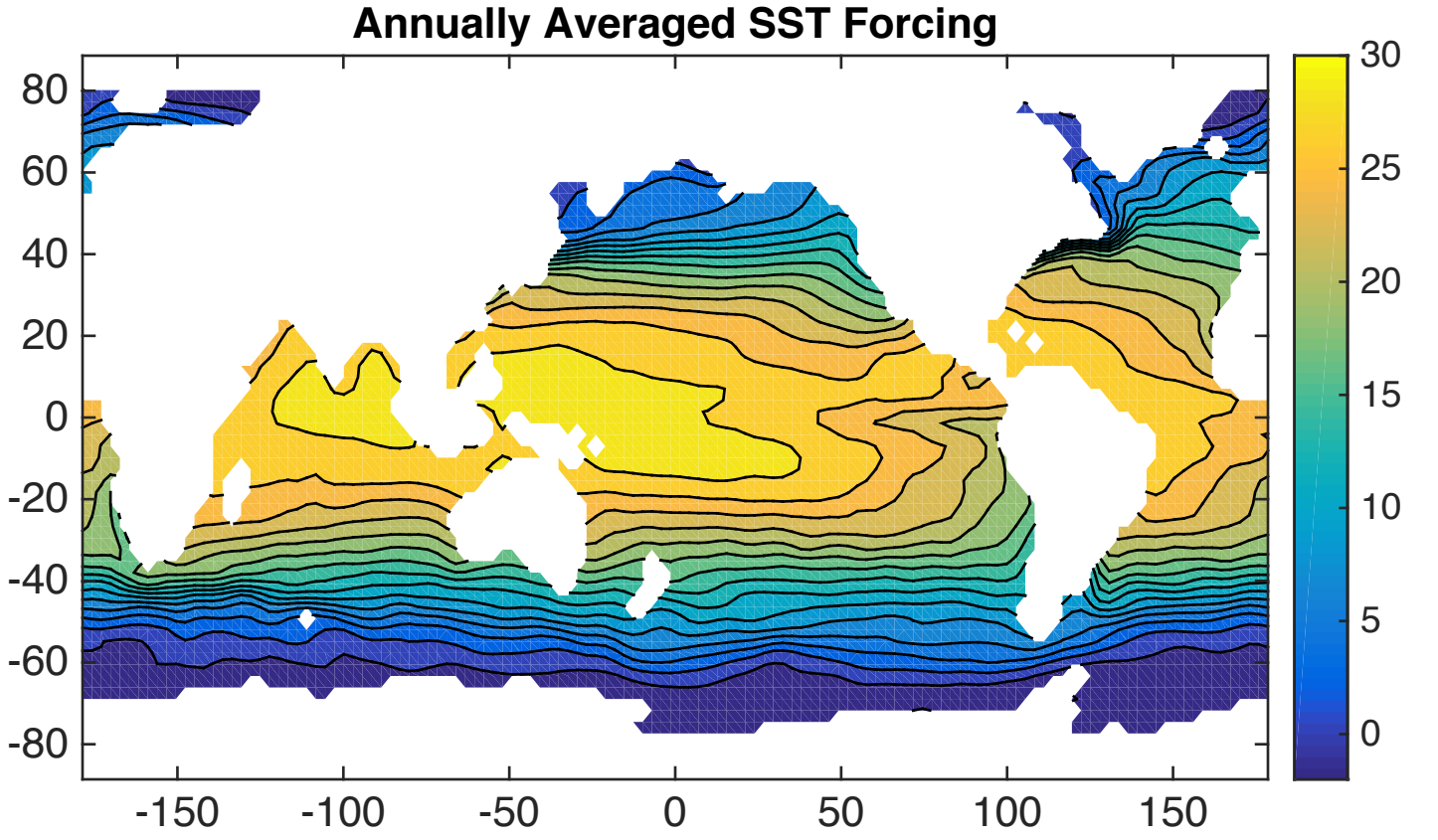
Annually Averaged SST Forcing
80
60
40
20
0
-20
-40
-60
-80
-150
-100
-50
0
50
100
150
30
25
20
15
10
5
0

Figure S1. Annual averages of a) Sea Surface Salinity (SSS) [g/kg] and b) Sea Surface Temperature (SST) [°C] surface forcing fields used in the model, as described in *Materials and Methods*. Contours in SSS are spaced at 0.3 g/kg; contours in SST are spaced at 2°C.

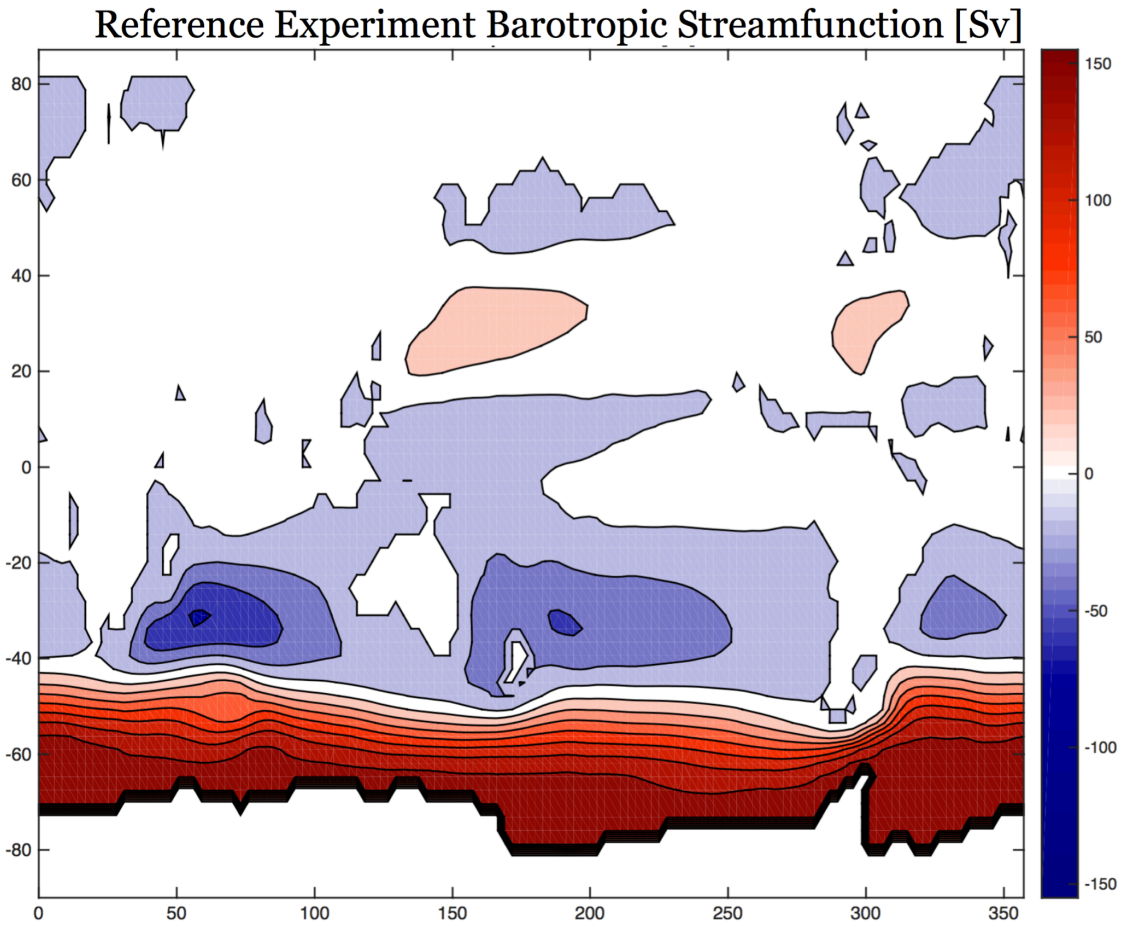

Figure S2. Barotropic streamfunction for the reference experiment (experiment *a*), the vertically-integrated analog of the overturning streamfunctions described in the main text. A strong ACC transport of 152 Sv is visible, as are the midlatitude gyres' transports of tens of Sv. Contours are at 20 Sv intervals.

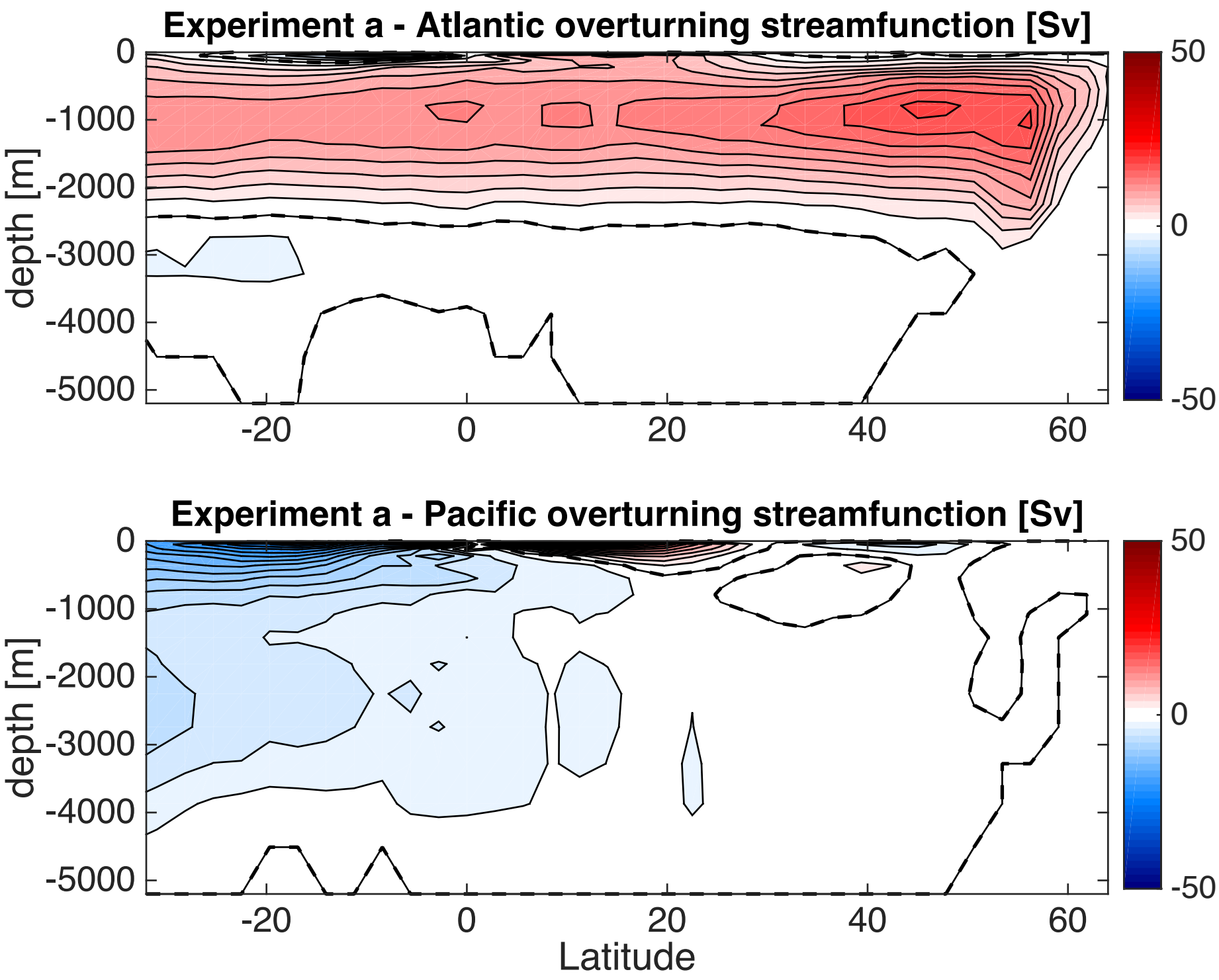
Experiment a - Atlantic overturning streamfunction [Sv]
depth [m]
0
-1000
-2000
-3000
-4000
-5000
-20
0
20
40
60
50
0
-50
Experiment a - Pacific overturning streamfunction [Sv]
depth [m]
0
-1000
-2000
-3000
-4000
-5000
-20
0
20
40
60
Latitude
50
0
-50

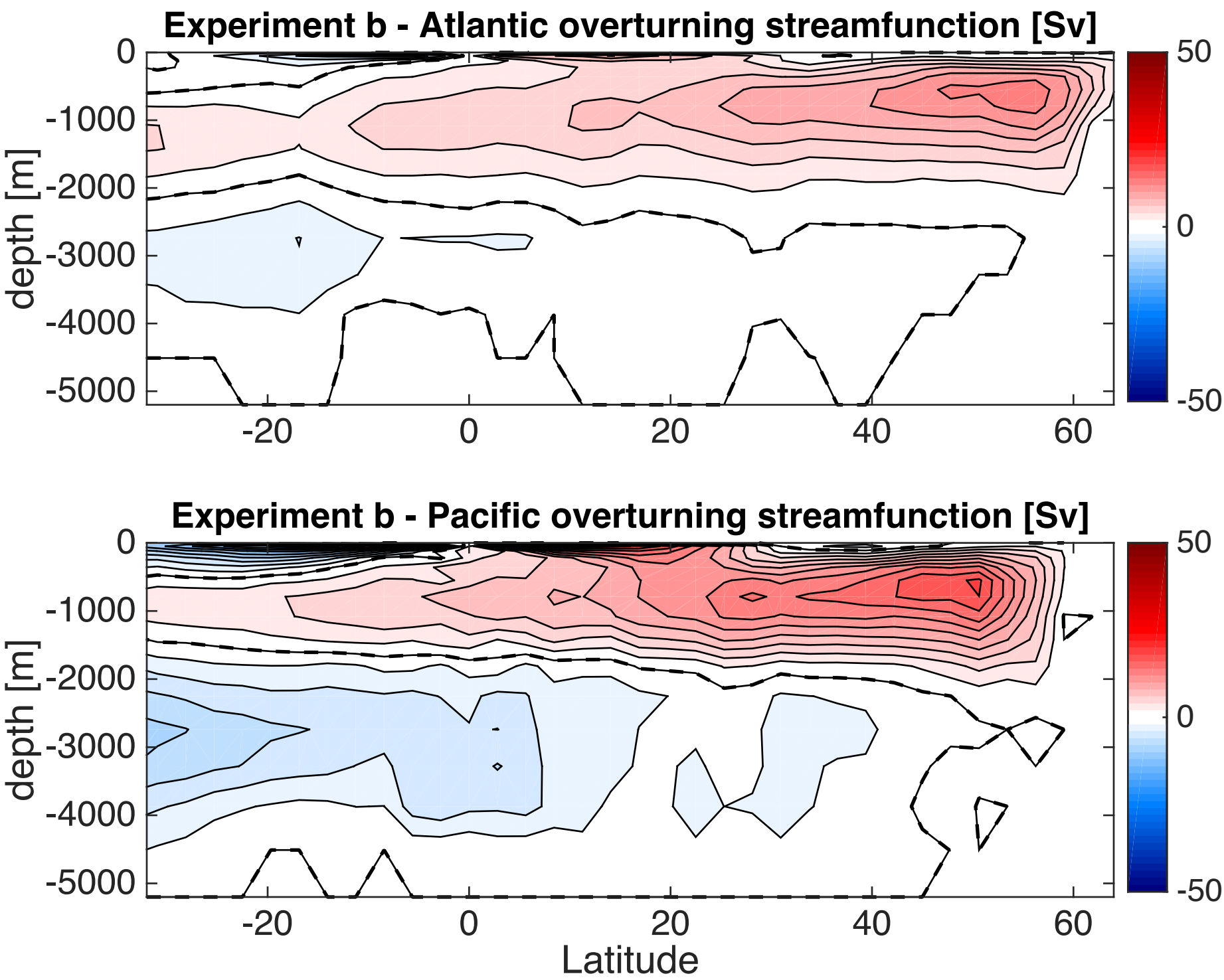
Experiment b - Atlantic overturning streamfunction [Sv]
depth [m]
0
-1000
-2000
-3000
-4000
-5000
-20
0
20
40
60
50
0
-50
Experiment b - Pacific overturning streamfunction [Sv]
depth [m]
0
-1000
-2000
-3000
-4000
-5000
-20
0
20
40
60
Latitude
50
0
-50

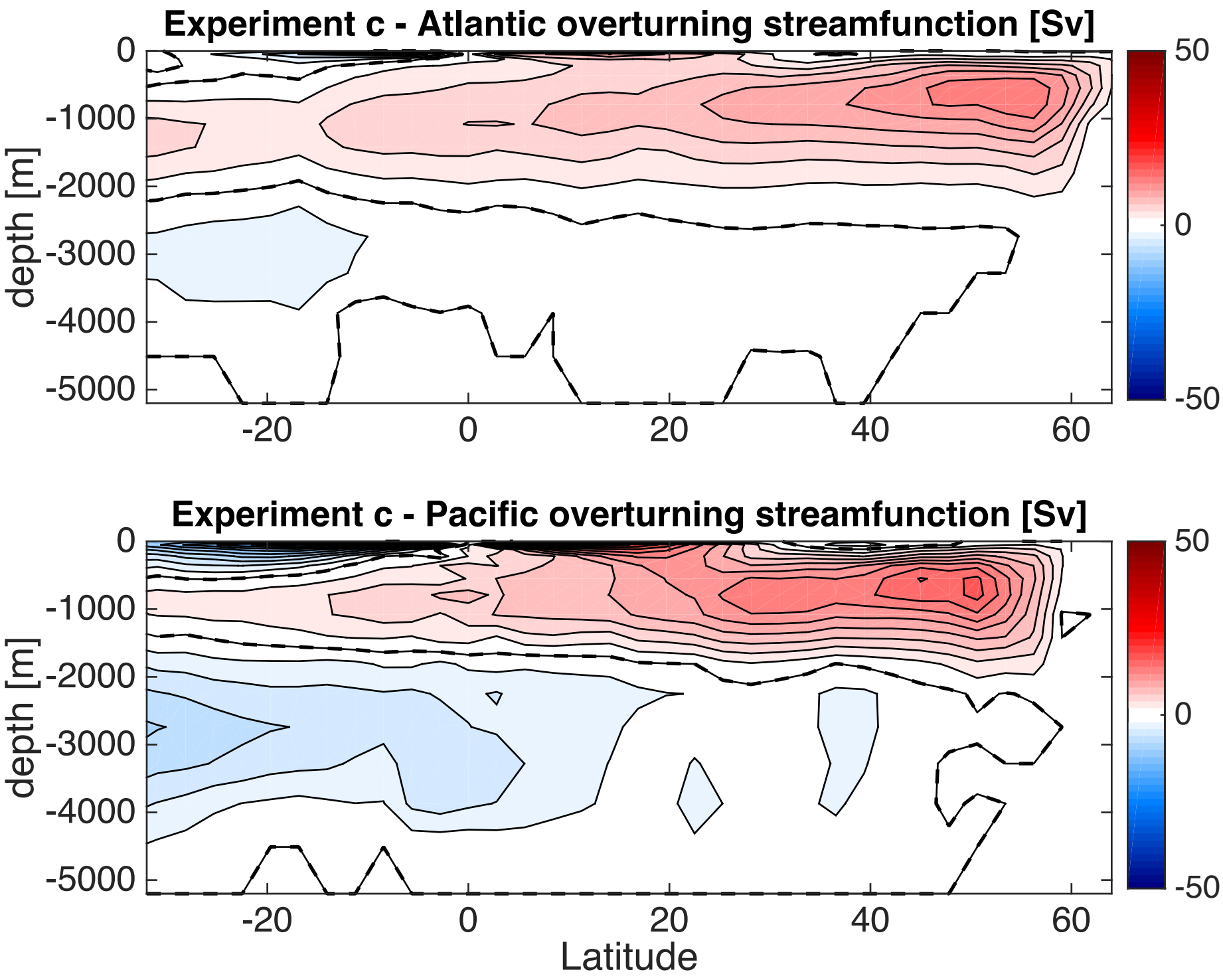
Experiment c - Atlantic overturning streamfunction [Sv]
depth [m]
0
-1000
-2000
-3000
-4000
-5000
-20
0
20
40
60
50
0
-50
Experiment c - Pacific overturning streamfunction [Sv]
depth [m]
0
-1000
-2000
-3000
-4000
-5000
-20
0
20
40
60
Latitude
50
0
-50

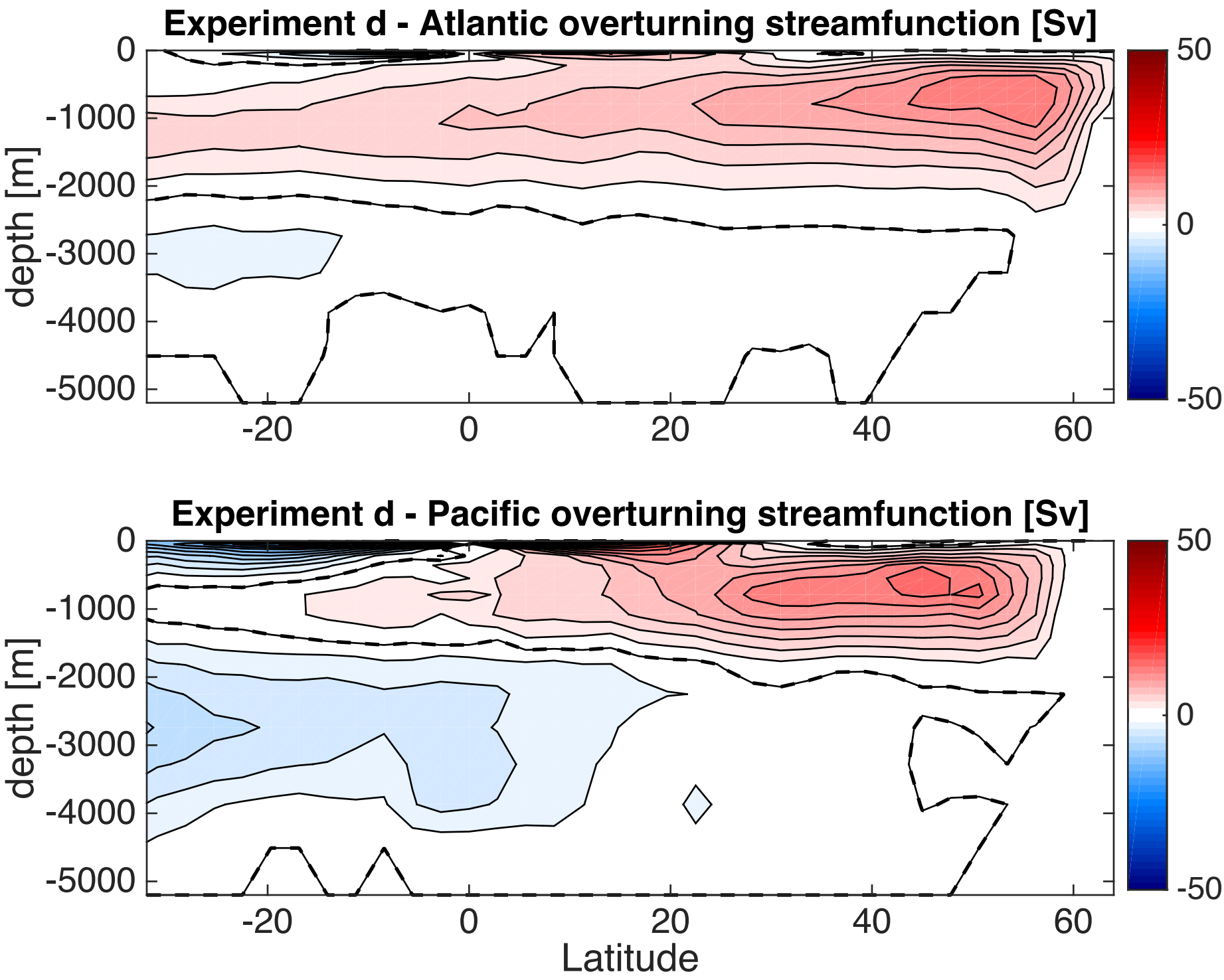
Experiment d - Atlantic overturning streamfunction [Sv]
depth [m]
0
-1000
-2000
-3000
-4000
-5000
-20
0
20
40
60
50
0
-50
Experiment d - Pacific overturning streamfunction [Sv]
depth [m]
0
-1000
-2000
-3000
-4000
-5000
-20
0
20
40
60
Latitude
50
0
-50

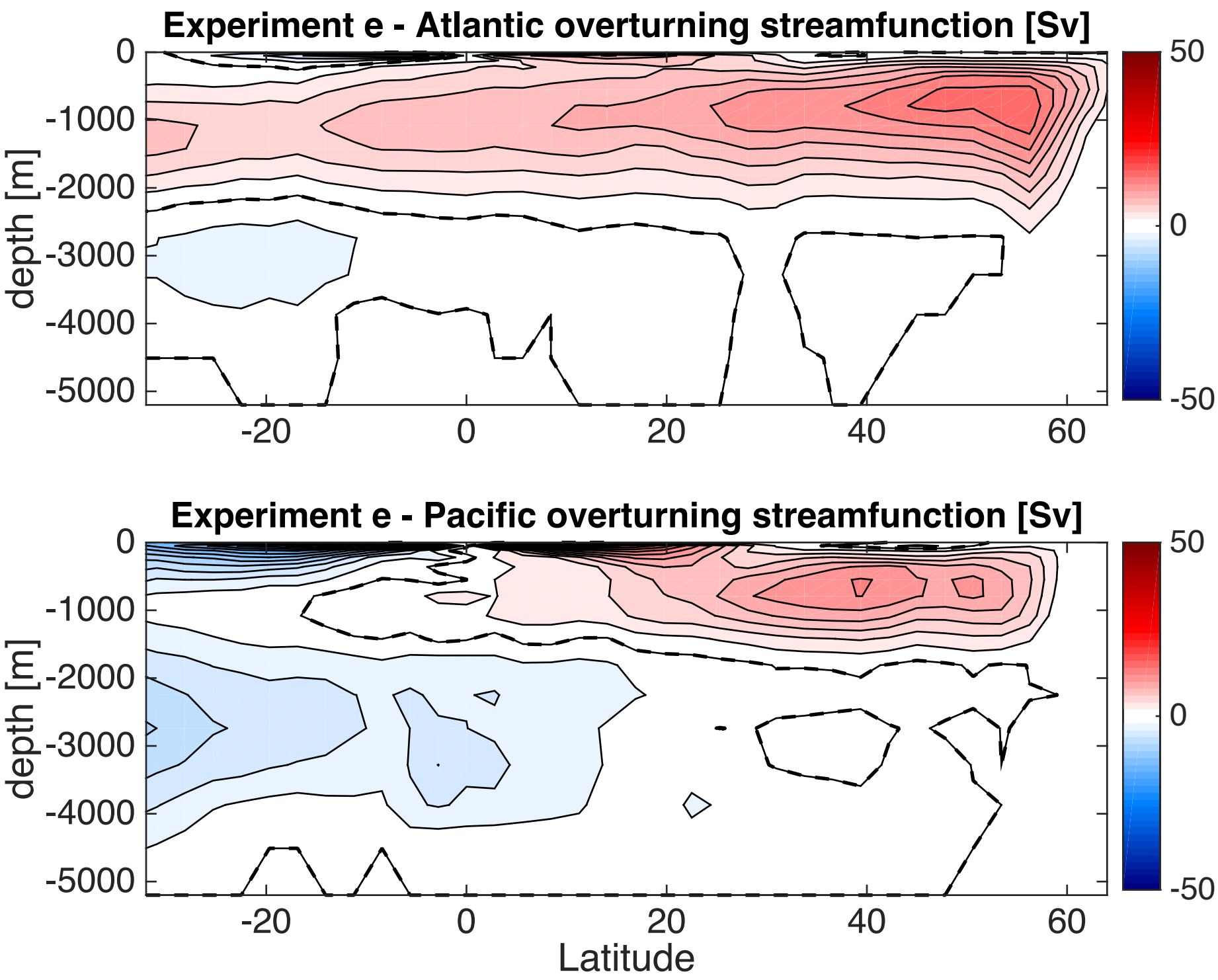
Experiment e - Atlantic overturning streamfunction [Sv]
0
-1000
-2000
-3000
-4000
-5000
depth [m]
-20
0
20
40
60
50
0
-50
Experiment e - Pacific overturning streamfunction [Sv]
0
-1000
-2000
-3000
-4000
-5000
depth [m]
-20
0
20
40
60
Latitude
50
0
-50

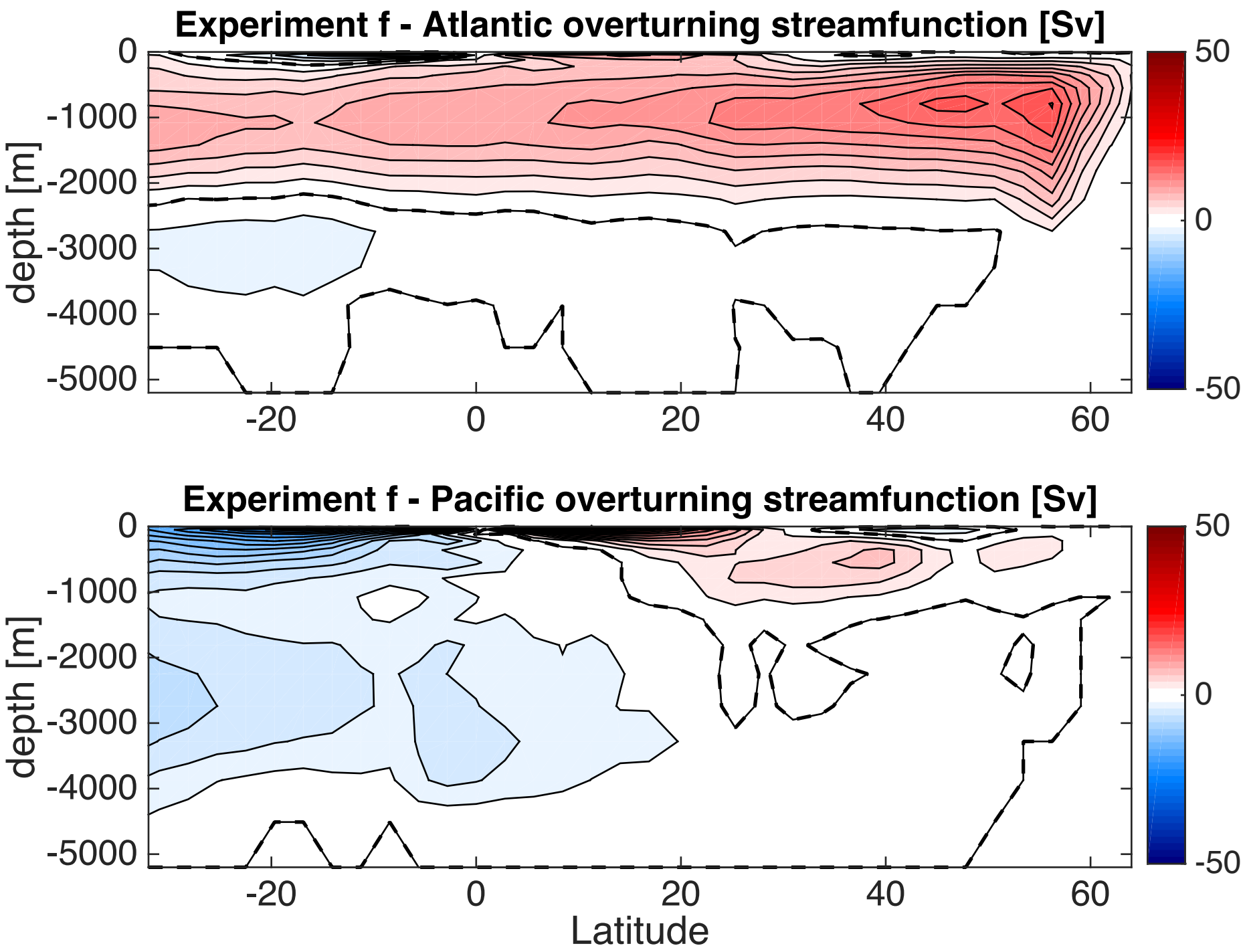
Experiment f - Atlantic overturning streamfunction [Sv]
depth [m]
0
-1000
-2000
-3000
-4000
-5000
-20
0
20
40
60
50
0
-50
Experiment f - Pacific overturning streamfunction [Sv]
depth [m]
0
-1000
-2000
-3000
-4000
-5000
-20
0
20
40
60
Latitude
50
0
-50

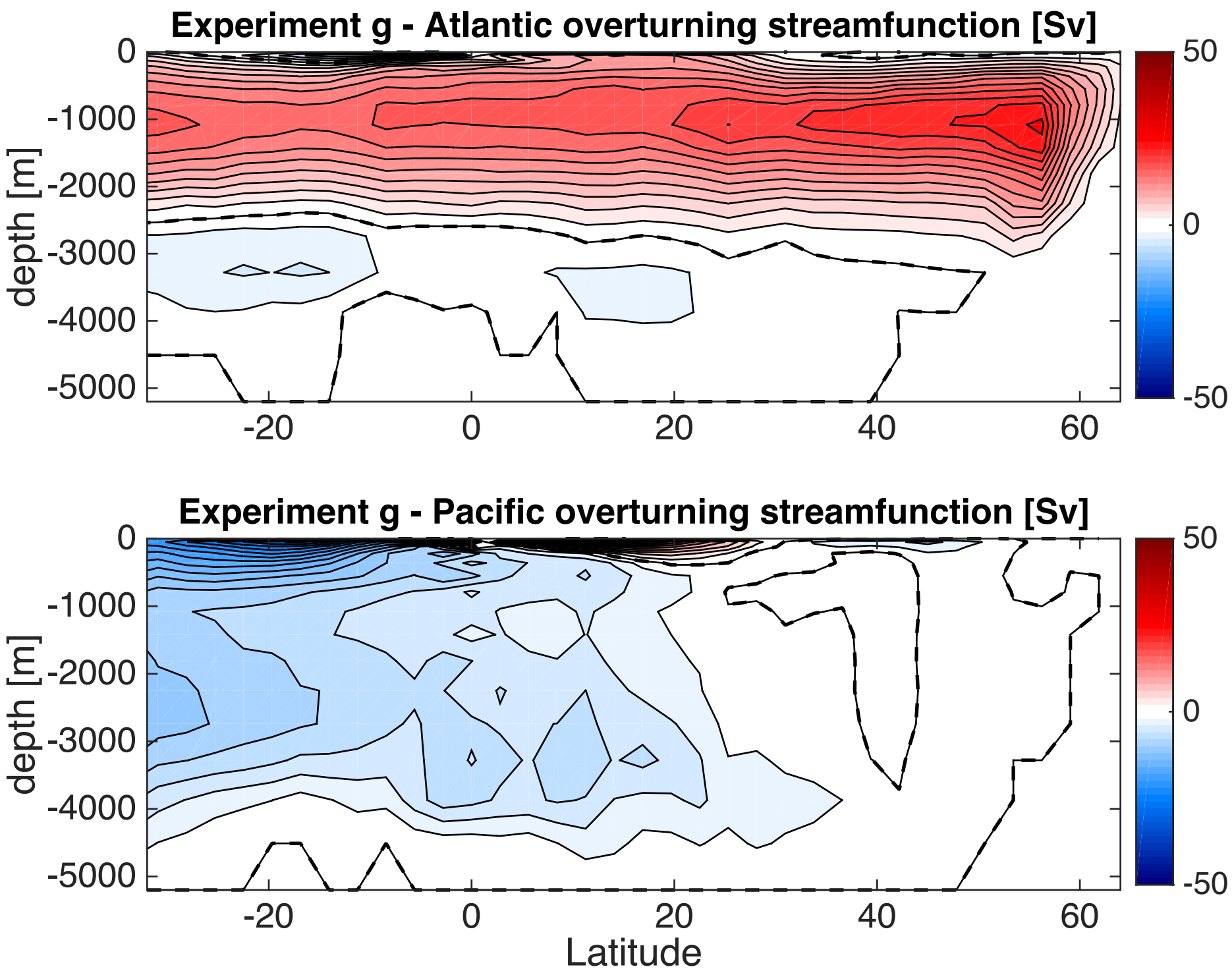
Experiment g - Atlantic overturning streamfunction [Sv]
depth [m]
0
-1000
-2000
-3000
-4000
-5000
-20
0
20
40
60
50
0
-50
Experiment g - Pacific overturning streamfunction [Sv]
depth [m]
0
-1000
-2000
-3000
-4000
-5000
-20
0
20
40
60
Latitude
50
0
-50

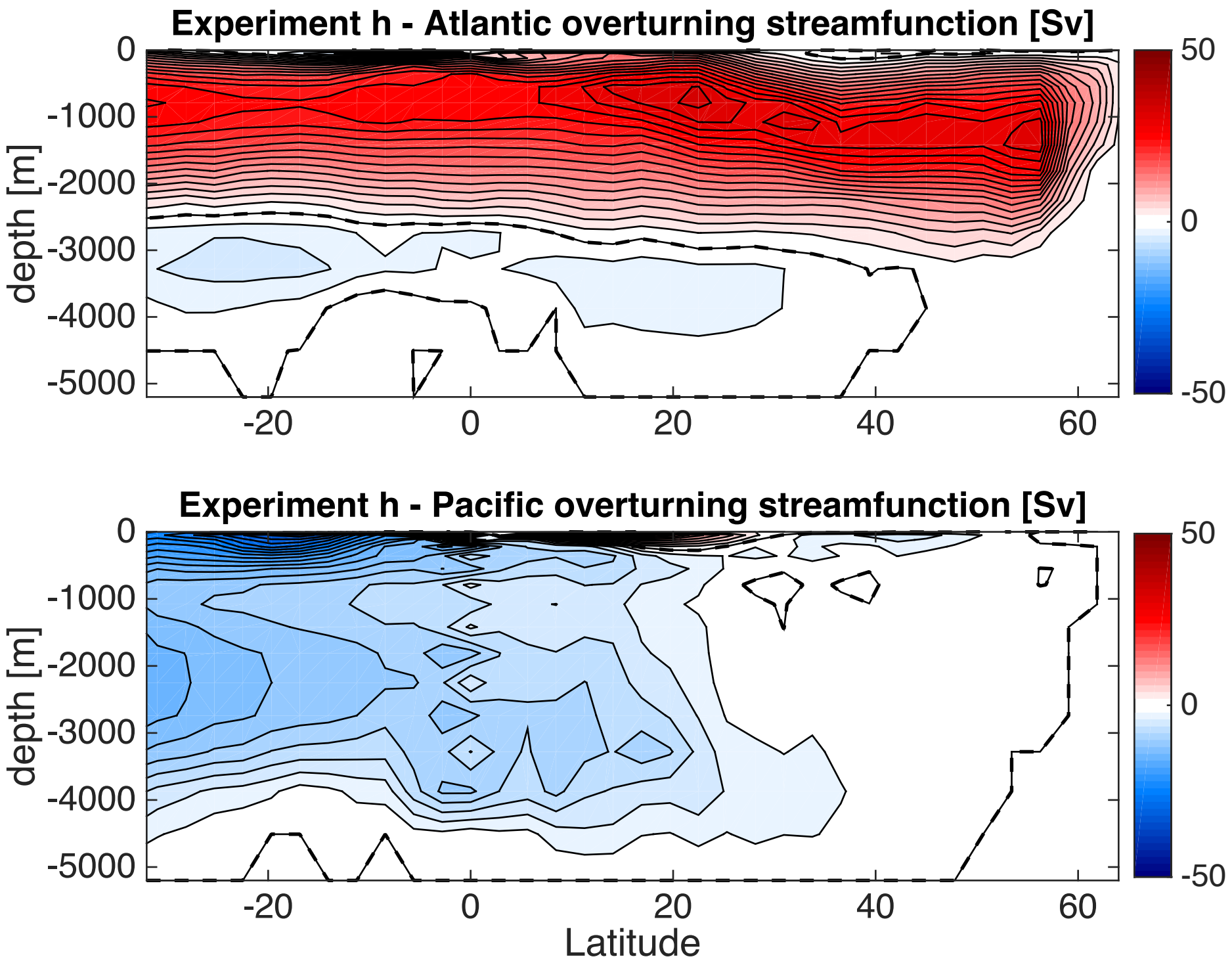
Experiment h - Atlantic overturning streamfunction [Sv]
depth [m]
0
-1000
-2000
-3000
-4000
-5000
-20
0
20
40
60
50
0
-50
Experiment h - Pacific overturning streamfunction [Sv]
depth [m]
0
-1000
-2000
-3000
-4000
-5000
-20
0
20
40
60
Latitude
50
0
-50

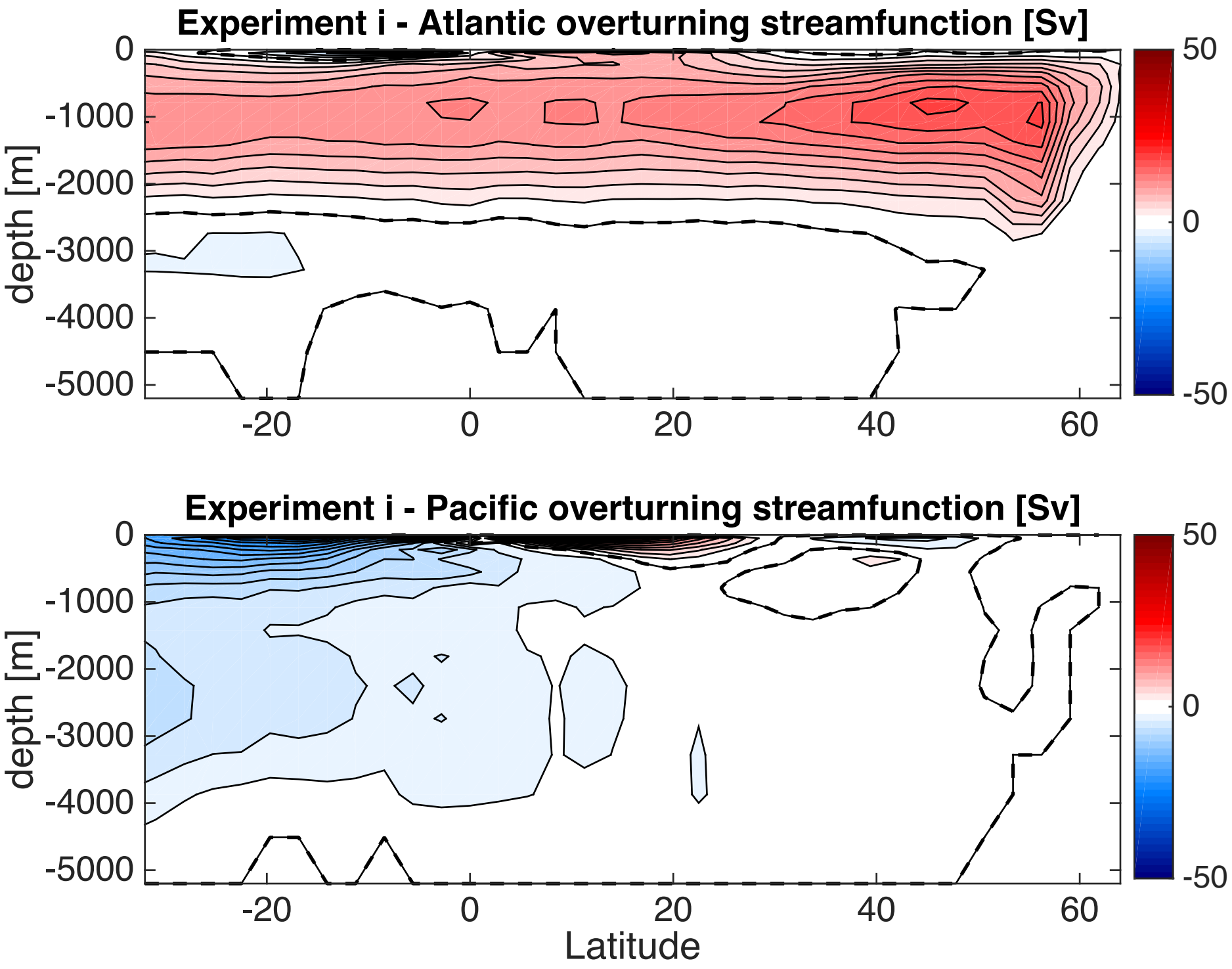
Experiment i - Atlantic overturning streamfunction [Sv]
depth [m]
0
-1000
-2000
-3000
-4000
-5000
-20
0
20
40
60
50
0
-50
Experiment i - Pacific overturning streamfunction [Sv]
depth [m]
0
-1000
-2000
-3000
-4000
-5000
-20
0
20
40
60
Latitude
50
0
-50

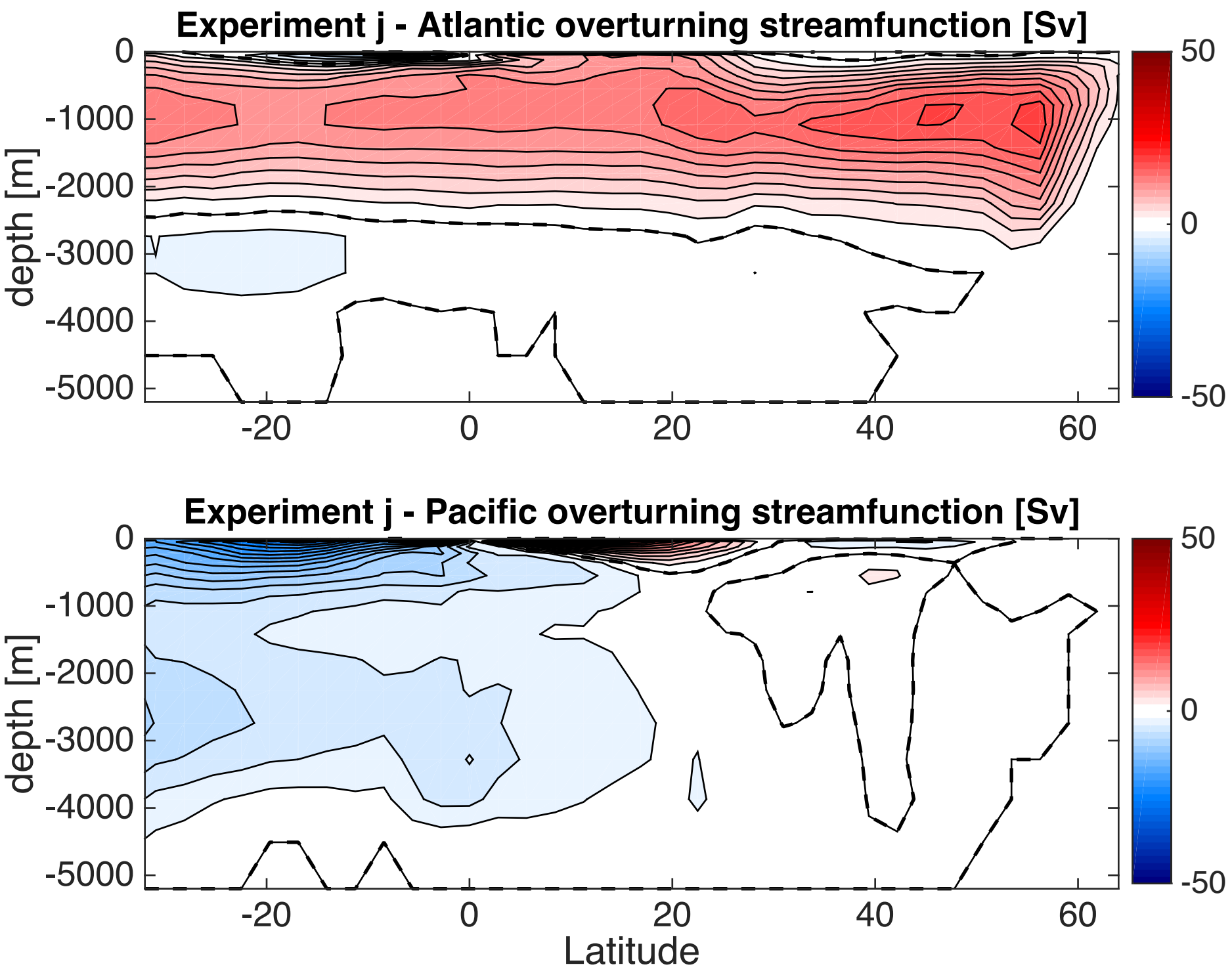
Experiment j - Atlantic overturning streamfunction [Sv]
0
-1000
-2000
-3000
-4000
-5000
depth [m]
-20
0
20
40
60
50
0
-50
Experiment j - Pacific overturning streamfunction [Sv]
0
-1000
-2000
-3000
-4000
-5000
depth [m]
-20
0
20
40
60
Latitude
50
0
-50

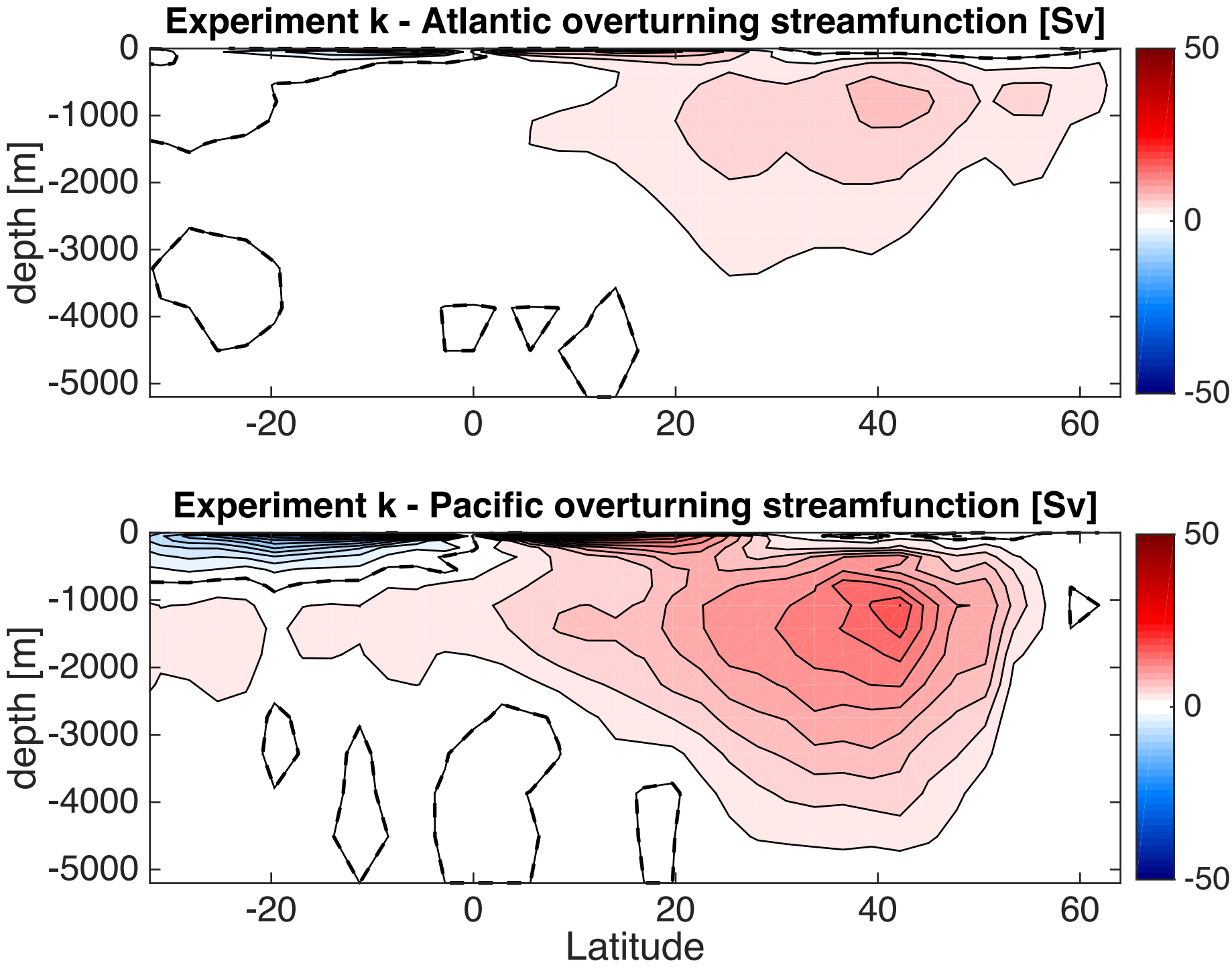
Experiment k - Atlantic overturning streamfunction [Sv]
depth [m]
0
-1000
-2000
-3000
-4000
-5000
-20
0
20
40
60
50
0
-50
Experiment k - Pacific overturning streamfunction [Sv]
depth [m]
0
-1000
-2000
-3000
-4000
-5000
-20
0
20
40
60
Latitude
50
0
-50

Figure S3. AMOC and PMOC for each experiment, as defined in the main text. Contours are spaced at 2 Sv; dashed line indicates the zero contour. For each subfigure the corresponding experiment is given in the figure title.

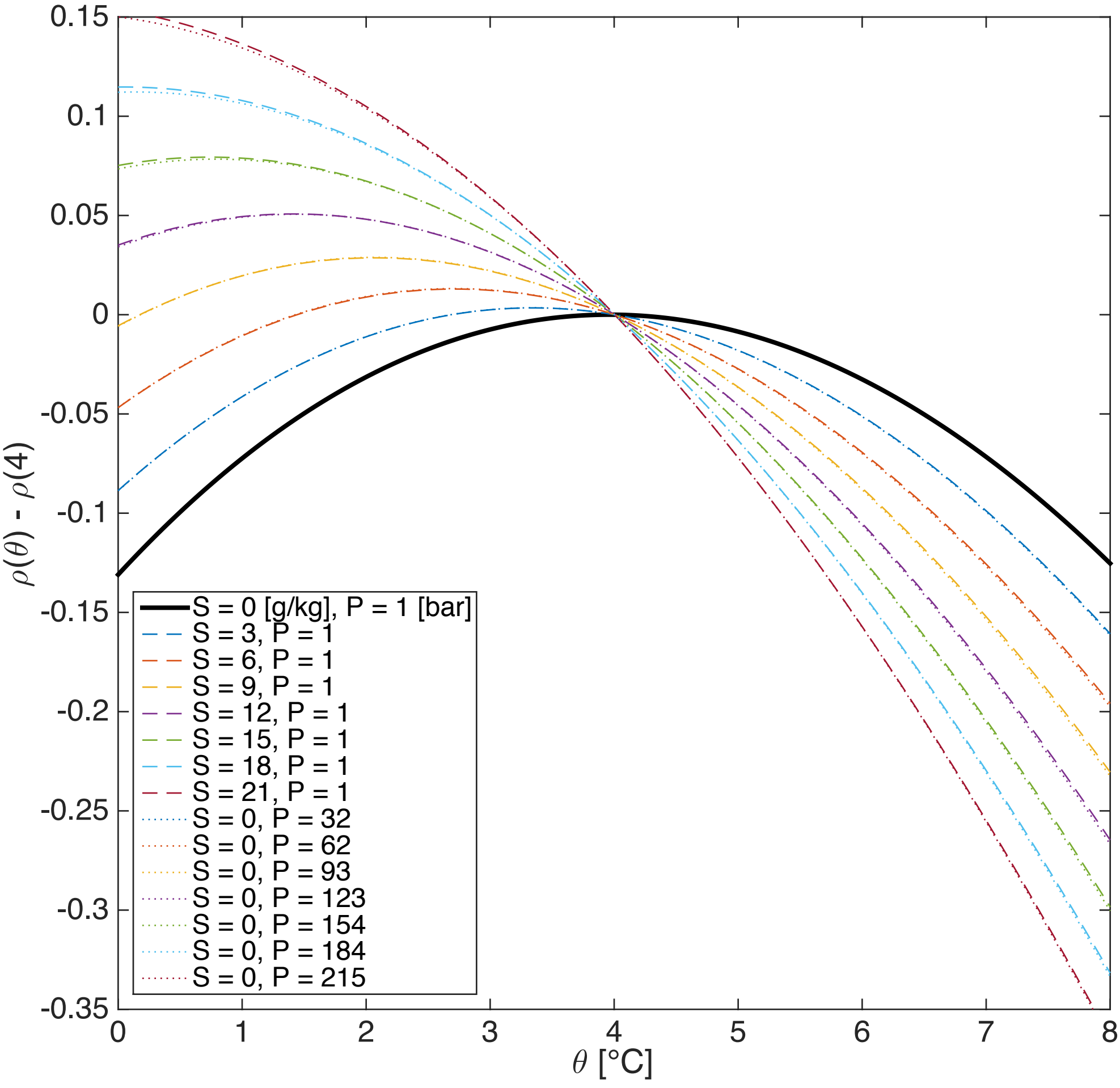
0.15
0.1
0.05
0
-0.05
-0.1
-0.15
-0.2
-0.25
-0.3
-0.35
0
1
2
3
4
5
6
7
8
$\rho(\theta)$ - $\rho(4)$
θ [°C]
S = 0 [g/kg], P = 1 [bar]
S = 3, P = 1
S = 6, P = 1
S = 9, P = 1
S = 12, P = 1
S = 15, P = 1
S = 18, P = 1
S = 21, P = 1
S = 0, P = 32
S = 0, P = 62
S = 0, P = 93
S = 0, P = 123
S = 0, P = 154
S = 0, P = 184
S = 0, P = 215

Figure S4. *In situ* density – potential temperature relationship for varying pressures and salinities. *In situ* density as a function of potential temperature θ, with $\rho(4)$ subtracted, for water with varying salinities at surface pressure (dashed lines) or with varying pressures at zero salinity (dotted lines). Note curves nearly overlap but not exactly, especially at low θ and high salinity or pressure

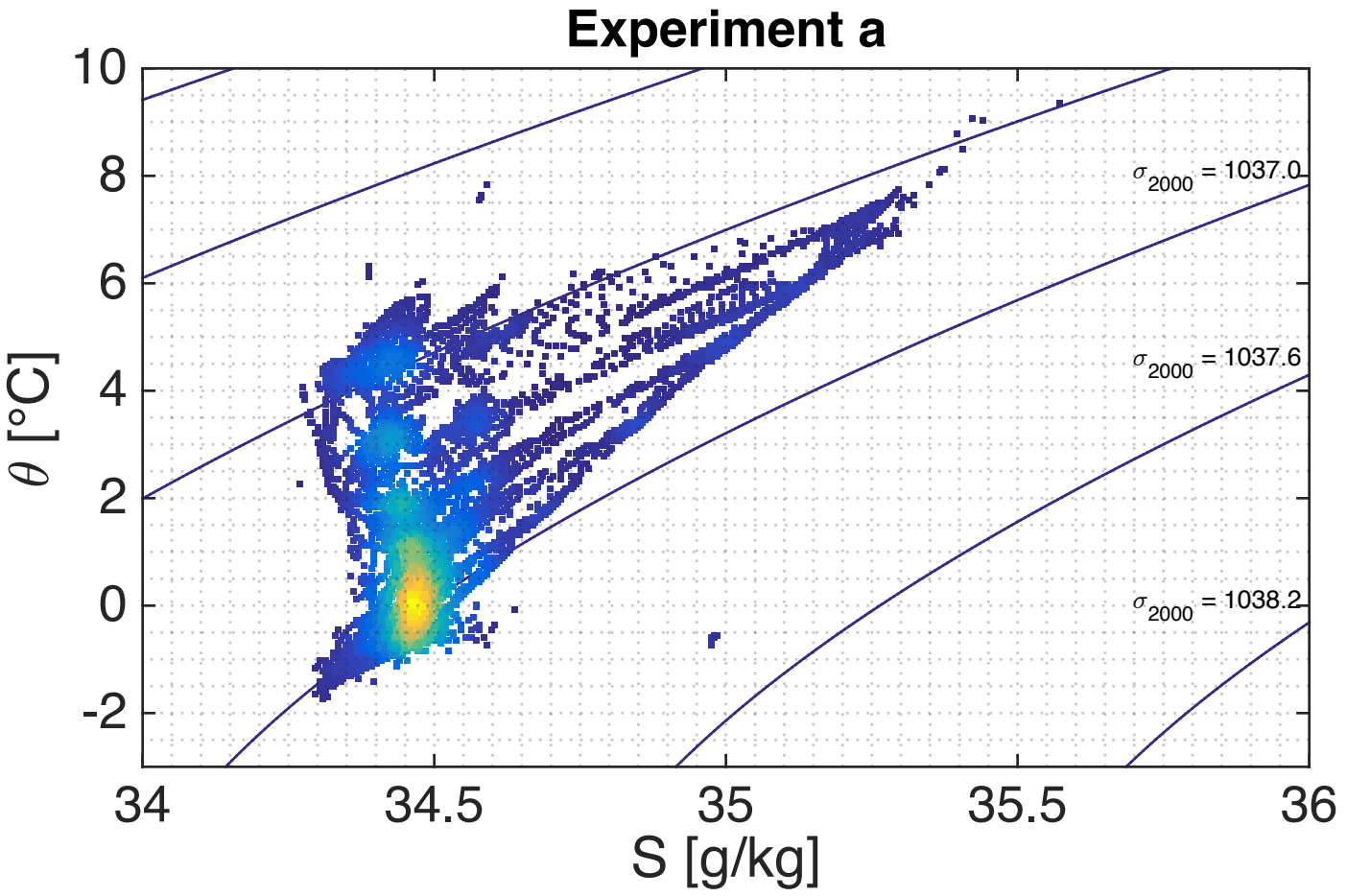
Experiment a
10
8
6
4
2
0
-2
θ [°C]
σ2000 = 1037.0
σ2000 = 1037.6
σ2000 = 1038.2
34
34.5
35
35.5
36
S [g/kg]

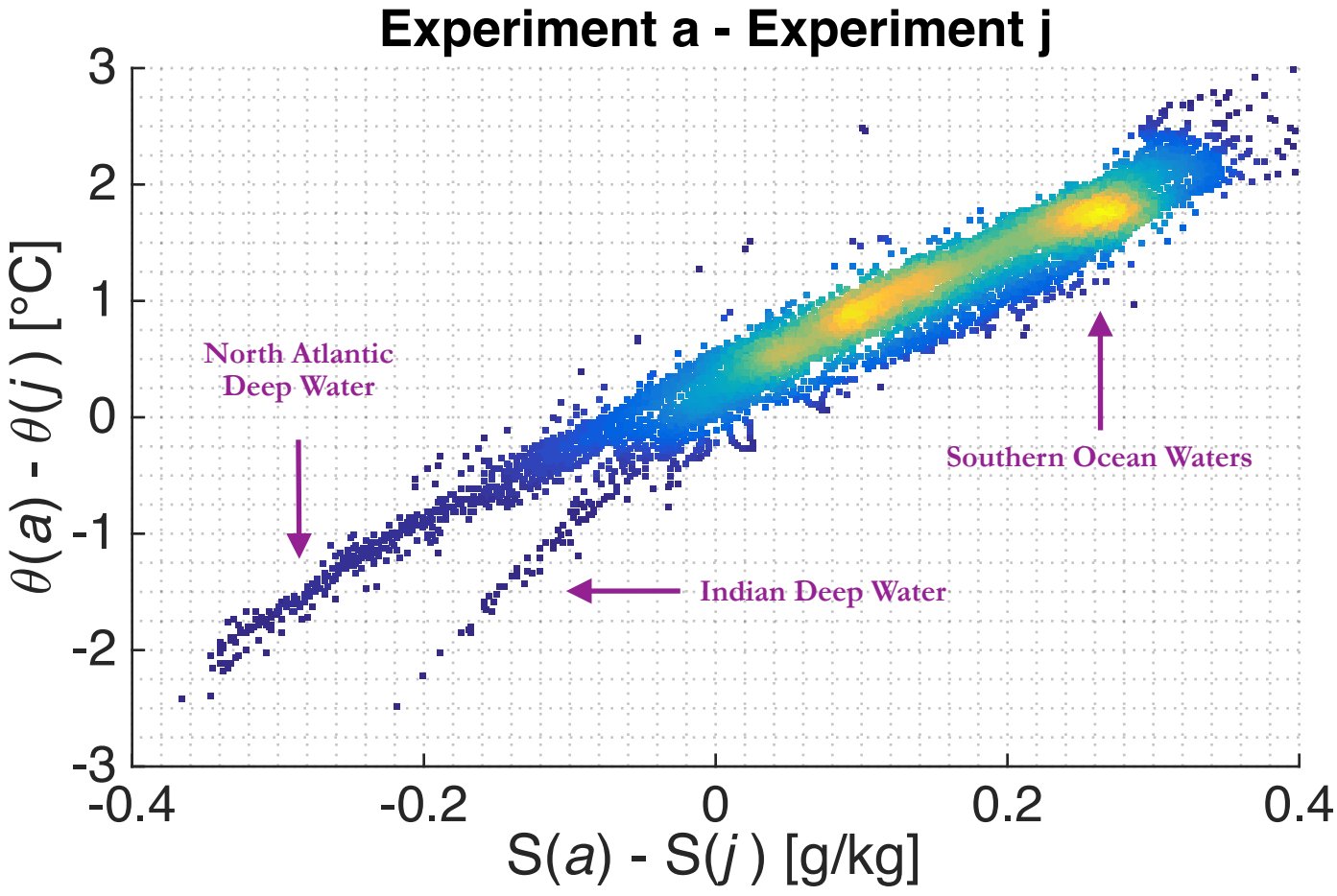
Experiment a - Experiment j
3
2
1
0
-1
-2
-3
θ(a) - θ(j) [°C]
North Atlantic
Deep Water
Southern Ocean Waters
Indian Deep Water
-0.4
-0.2
0
0.2
0.4
S(a) - S(j) [g/kg]

Figure S5. a) For each model gridpoint below 1 km depth, the experiment *a* equilibrium time-mean potential temperature and salinity are scattered, colored by the local density of scattered points. Potential density contours are referenced to 2000 dbar and spaced at 0.6 kg m^{-3} as a guide. b) For each model gridpoint below 1 km depth, the difference between experiments *a* and *j* in the equilibrium time-mean potential temperature and salinity are scattered, colored by the local density of points. Individual water masses with characteristic differences between the two experiments are labeled (e.g. waters in the Southern Ocean below 1 km depth are ~0.3 g/kg saltier and ~1.8°C colder in experiment *a* than in experiment *j*).